Lattice dynamics of neodymium: Influence of 4*f* electron correlations

O. Waller,[1,2,*] P. Piekarz,[3,†] A. Bosak,[4] P. T. Jochym,[3] S. Ibrahimkutty,[1,2,‡] A. Seiler,[1,2]
M. Krisch,[4] T. Baumbach,[1,2,5] K. Parlinski,[3] and S. Stankov[1,2,§]

[1]*Laboratory for Applications of Synchrotron Radiation, Karlsruhe Institute of Technology, D-76131 Karlsruhe, Germany*
[2]*Institute for Photon Science and Synchrotron Radiation, Karlsruhe Institute of Technology, D-76344 Eggenstein-Leopoldshafen, Germany*
[3]*Institute of Nuclear Physics, Polish Academy of Sciences, PL-31342 Kraków, Poland*
[4]*ESRF–The European Synchrotron, F-38000 Grenoble, France*
[5]*ANKA, Karlsruhe Institute of Technology, D-76344 Eggenstein-Leopoldshafen, Germany*

(Received 25 November 2015; revised manuscript received 6 June 2016; published 5 July 2016)

Incorporation of strong electron correlations into the density functional theory (DFT) for the electronic structure calculations of light lanthanides leads to a modification of interatomic forces and consequently the lattice dynamics. Using first-principles theory we demonstrate the substantial influence of the 4*f* electron correlations on the phonon dispersion relations of Nd. The calculations are verified by an inelastic x-ray scattering experiment performed on a single-crystalline Nd(0001) film. We show that very good agreement between the calculated and measured data is achieved when electron-electron interactions are treated by the DFT+*U* approach.

DOI: 10.1103/PhysRevB.94.014303

Achieving a correct description of materials with open and highly localized *d* and *f* shells (strongly correlated materials) by density functional theory (DFT) remains among the most challenging tasks in theoretical condensed matter physics [1]. Over the past about five decades DFT has been spectacularly successful in calculating material properties as well as designing novel materials with superior characteristics [2,3]. For many elements and compounds, the exchange-correlation functionals required for DFT calculations can be satisfactorily described using the local density approximation (LDA), or generalized gradient approximation (GGA) achieving very good agreement with experimental data [4,5]. These standard approximations, however, fail to describe strongly correlated systems because of uncompensated self-interactions that introduce large errors. Consequently, the localized states in Mott insulators, or *f* electron systems cannot be properly treated within the LDA or GGA. To overcome these problems several methods have been proposed to improve the electron potentials by taking into account their dependence on orbital occupation. The most effective and accurate methods are self-interaction corrected LDA [6], LDA+*U* [7], hybrid functional method [8], dynamical mean field theory (DMFT) [9], and reduced density matrix functional theory (RDMFT) [10]. The combination of DFT and DMFT [11] has recently been proven to be a particularly suitable approach for treating the strong electron-electron interactions in 3*d*, 4*f*, and 5*f* elements and compounds [12], exhibiting nevertheless some limitations [13]. In spite of its success and continuous development, the DFT+DMFT remains a computationally expensive and demanding method.

The frequencies of lattice vibrations are determined by the interatomic forces and constitute a sensitive data set for verification of computational models. In strongly correlated systems, the DFT calculations often fail to correctly describe the phonon energies and experimentally observed phonon anomalies [14]. In many cases the improvement of density functionals results in a better description of the lattice dynamics in transition-metal oxides [15–19], actinide compounds [20], and rare-earth oxides [21].

Currently there is an increasing need for reliable predictive calculations of the lanthanides and their compounds as this class of materials is of great interest for both fundamental research and modern technology. The lanthanides are characterized by occupation of the 4*f* shell and exhibit strong electron correlations, complex magnetic order, and in some cases large spin-orbit interactions that constitute a formidable challenge for theoreticians. In the *standard approach* the 4*f* electrons are treated as core states, and for the heavy rare earths (Gd–Lu) this approximation reproduces many physical properties [22–24]. When going from the heavy to the light lanthanides (Ce–Sm), however, the disagreement between theory and experiment gradually increases due to the more delocalized nature of the 4*f* electrons [24]. A continuous improvement in the calculation of electronic and structure properties of rare-earth metals was achieved using the above-mentioned approaches [25–28]. Despite these efforts, a systematic study of the influence of the 4*f* electron correlations on the lattice dynamics of the light lanthanides has not been performed so far.

The experimental investigation of pure lanthanides is also a demanding task because of difficulties in obtaining single crystals of high quality and purity, high oxidation ability, and in some cases large absorption cross sections for thermal neutrons. Due to these obstacles the lattice dynamics of some of the 4*f* elements has not yet been determined despite decades of research. A successful experimental approach is to produce high quality single-crystalline films by molecular beam epitaxy and to perform the experiments *in situ* [29,30] or, as demonstrated here, *ex situ* after covering the film by a protective layer.

In this paper we investigate the influence of the 4*f* electron correlations on the lattice dynamics of light lanthanide neodymium (Nd). The results from DFT calculations are

*Present address: Polytechnique Montréal, Montréal, Québec H3C 3A7, Canada.
†Przemyslaw.Piekarz@ifj.edu.pl
‡Present address: Max Planck Institute for Solid State Research, D-70569 Stuttgart, Germany.
§Svetoslav.Stankov@kit.edu

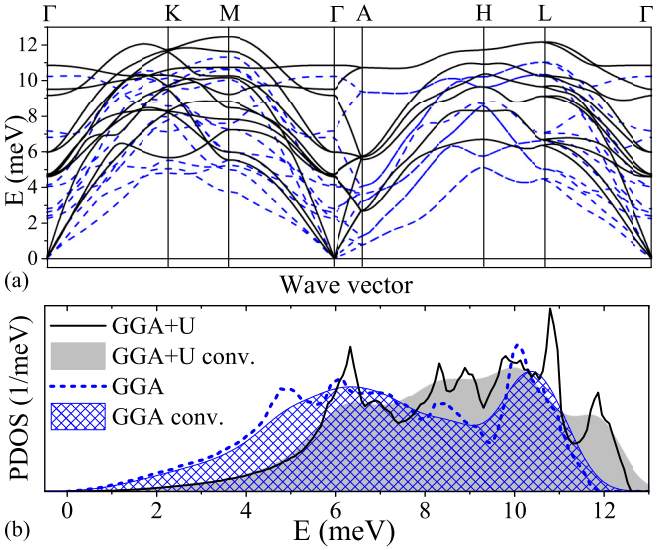

FIG. 1. *Ab initio* calculated (a) dispersion relations and (b) PDOS of Nd within GGA and GGA+U using the optimized lattice constants. The high-symmetry points in units of $2\pi/a$ are $\Gamma = (0,0,0)$, $K = (\frac{1}{3},\frac{1}{3},0)$, $M = (\frac{1}{2},0,0)$, $A = (0,0,\frac{1}{2})$, $H = (\frac{1}{3},\frac{1}{3},\frac{1}{2})$, and $\mathrm{L} = (\frac{1}{2},0,\frac{1}{2})$. Shaded areas correspond to the Gauss convolution with FWHM = 1 meV.

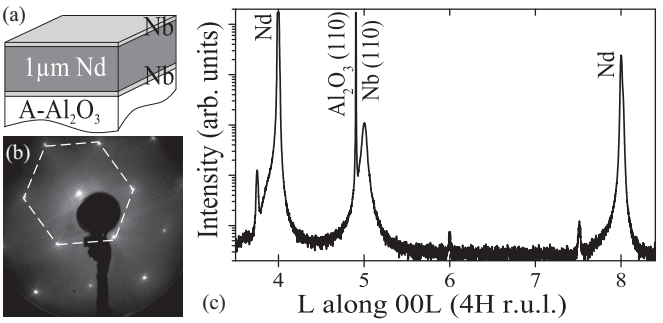

FIG. 2. (a) Schematic presentation of the investigated sample. (b) LEED image (obtained at 100 eV) of the Nd(0001) surface. The hexagonal ab plane is indicated by broken white lines. (c) XRD scan along $00L$ in dhcp $4H$ reciprocal lattice units.

compared to phonon dispersions measured by inelastic x-ray scattering (IXS) on a Nd(0001) film. We demonstrate that GGA+U, being the simplest approach for including local electron correlations, results in a very good agreement with experiment.

The DFT calculations were performed using the VASP code [31]. The electron wave functions and charge density were optimized by solving the Kohn-Sham equations within the projector augmented-wave method [32] and generalized gradient approximation [33]. The local interactions between the $4f$ valence electrons were included within the GGA+U method [7] with the Coulomb parameter $U = 4.8$ eV and Hund's exchange $J = 0.6$ eV taken from constrained random-phase approximation studies [34]. The results obtained with the GGA+U are compared to calculations with $4f$-band (standard GGA) and with $4f$-core (GGA_0) electron potentials. We assumed a ferromagnetic order with the optimized magnetic moments equal to $3.4\mu_B$ and investigated the effect of spin-orbit coupling (SOC) on the lattice parameters and phonon energies. We used the controlled symmetry reduction method to eliminate metastable states in the GGA+U calculations [35].

Different approximations were tested using the double hcp (dhcp) primitive cell (space group $P6/mmc$) with four Nd atoms. The reciprocal space was sampled with an $8 \times 8 \times 8$ k-point Monkhorst-Pack grid [36] and an energy cutoff of 320 eV, which resulted in well converged values of the total energy and lattice parameters. The bulk modulus, its derivative, and the elastic constants were determined at the theoretical equilibrium volumes using the stress-strain approach [37].

The phonon calculations were performed within the direct method implemented in the PHONON software [38] used previously for lattice dynamics studies of Eu [29] and Sm [30]. The Hellmann-Feynman forces and force constants were obtained by displacing atoms from the equilibrium positions in the 32-atom supercell. The k-point sampling was reduced to a $4 \times 4 \times 4$ grid. The number and directions of necessary displacements were determined by the hexagonal symmetry constraints. The phonon dispersions and polarization vectors were obtained by diagonalization of the dynamical matrix. The dispersion relations along high-symmetry directions and phonon density of states (PDOS) obtained with the optimized lattice parameters [39] are presented in Fig. 1.

A high quality single-crystalline Nd(0001) film was prepared following the growth protocol established by Dufour *et al.*, [40]. An epi-polished, A-plane $Al_2O_3(11\bar{2}0)$ substrate was subjected to a solvent degrease process followed by annealing at 1273 K for 1 h in a UHV chamber with a base pressure of 3×10^{-11} mbar. A 30-nm-thick Nb(110) buffer layer was deposited at 1223 K on the substrate. Metallic Nd (supplied by the Ames Laboratory) with a purity of 99.99% was deposited on the Nb(110) layer. The substrate temperature was elevated during deposition to 873 K to enhance surface mobility, necessary for the formation of the Nd(0001) film with a thickness of about 1 μm [Fig. 2(a)]. The low-energy electron diffraction (LEED) image in Fig. 2(b) reveals the formation of an atomically flat Nd(0001) surface with a hexagonal symmetry. Figure 2(c) plots the x-ray diffraction (XRD) scan measured after covering the sample with a 20-nm-thick Nb layer to avoid oxidation. The data analysis confirmed the formation of a high quality and purity single-crystalline Nd(0001) film with a negligible amount of polycrystalline phases. The c-lattice constant (11.796 Å) of the Nd sample determined from the XRD measurement is in very good agreement with the published data (Table I).

The IXS experiment [41] was performed at the beamline ID28 of the European Synchrotron (ESRF) with an energy resolution of 3.0 meV (full width at half maximum) at a photon energy of 17.794 keV. During the measurement the sample was kept at room temperature in a vacuum of 5×10^{-6} mbar. The experiment was performed in grazing incidence geometry at an incidence angle of 0.4°. Due to this experimental constraint the phonon branches with both transverse and longitudinal polarizations were measured close to the directions $\Gamma \rightarrow K \rightarrow M$ and $\Gamma \rightarrow M \rightarrow \Gamma$ with an offset in the z direction. Along $\Gamma \rightarrow A$, the branches with longitudinal polarization were measured without an offset. A

TABLE I. Lattice constants (a,c), volume per one atom (V), and thermoelastic properties (bulk modulus B, derivative of the bulk modulus B', elastic constants c_{xy}, and lattice specific heat C_V at 300 K) of Nd.

Property	GGA_0	GGA	GGA+U(SOC)	Expt.
a (Å)	3.690	3.528	3.669 (3.670)	3.658[a]
c (Å)	11.870	11.277	11.804 (11.824)	11.797[a]
V (Å^3/atom)	34.997	30.389	34.398 (34.470)	34.18[a]
B (GPa)	34.7	18.6	31.4 (32.15)	31.8[a]
B' (GPa)	3.09	2.41	3.05 (3.04)	2.9[b]
c_{11} (GPa)	59.9	31.4	55.2	58.78[c]
c_{33} (GPa)	72.2	39.1	65.1	65.13[c]
c_{12} (GPa)	29.8	14.9	27.9	24.58[c]
c_{13} (GPa)	16.5	11.1	14.2	16.20[c]
c_{44} (GPa)	18.8	6.3	18.5	16.20[c]
C_V (J/mol K)	24.67	24.75	24.69	24.68[d]

[a]Reference [42].; [b]Reference [43].; [c]Reference [44].; [d]Reference [45].

list of the measured branches is given in Table II. The phonon energies were obtained by fitting a model function composed of a sum of Lorentzian profiles to the experimental data.

A comparison of the calculated and experimentally determined lattice constants (Table I) reveals a strong effect of the local Coulomb interaction U and a rather minor influence of the SOC. While GGA underestimates the experimental lattice constants by about 4%, GGA+U results in an agreement of better than 0.1%. This shows that the interaction terms with U and J introduce relevant corrections to the atomic bonding. The bulk modulus and elastic constants obtained within GGA+U are in very good agreement with the available experimental data (Table I). The effect of SOC on the bulk modulus and its derivative is very weak. As already shown in previous studies [24,28], the structural and elastic parameters obtained within the $4f$-core model GGA_0 are overestimated exhibiting, however, better agreement with experiment than the $4f$-band GGA calculations, which significantly underestimate the bulk modulus [28].

A comparison of the dispersion relations calculated with GGA and GGA+U [Fig. 1(a)] reveals a remarkable shift of the phonon branches to higher energies for GGA+U. A splitting of the high-energy modes results in an effective broadening of the PDOS that is clearly visible in Fig. 1(b) [46]. The increase of interatomic forces originates from the implemented local Coulomb and exchange interactions. Apparently, the origin of this result is the modification of electronic properties, namely, an enhanced localization of the $4f$ electrons, consequently a reduced screening obtained by the GGA+U. This results in augmented interatomic forces compared to the GGA values, despite the larger lattice constants obtained by the latter.

TABLE II. Direction, polarization [longitudinal acoustic/optic (LA/LO), transverse acoustic/optic (TA/TO)], and exact coordinates of the measured phonon branches in reciprocal lattice units.

Direction	Mode	Momentum transfer
$\Gamma \rightarrow$ K $\rightarrow M$	LA/LO	[1+q 1+q 0.2] ($0.1 \leqslant q \leqslant 0.5$)
	TA/TO	[3−q −3−q 0.3] ($0.1 \leqslant q \leqslant 0.5$)
$\Gamma \rightarrow$ A	LA/LO	[0 0 2 +q] ($0 \leqslant q \leqslant 1.6$)
$\Gamma \rightarrow M \rightarrow \Gamma$	LA/LO	[2+q −2−q 0.2] ($0.1 \leqslant q \leqslant 0.9$)
	TA/TO	[1−q 1+q 0.2] ($0.6 \leqslant q \leqslant 1.8$)

The experimental phonon dispersions were obtained with an offset in the z direction due to the employed grazing incidence scattering geometry, and they cannot be directly compared with the calculations presented in Fig. 1(a). Therefore, GGA+U calculations were performed for the exact experimental directions (Table II) and compared with the experimental points in Fig. 3. In order to identify the most intense phonon branches, the dynamical form factor was calculated [39,41] and presented in color scale. Close to the directions $\Gamma \rightarrow K \rightarrow M$ and $\Gamma \rightarrow M \rightarrow \Gamma$ for both longitudinal [Figs. 3(a) and 3(d)] and transverse [Figs. 3(b) and 3(e)] polarizations, the experimental points coincide with the calculated branches of highest intensities with an average deviation of 6.5%. Attribution of the experimental points to close-lying branches is limited by the experimental energy resolution. This is, for example, visible in Fig. 3(e) where at $q = 1.7$ the experimental point appears between two close-lying branches of similar intensity and separated by less than 2 meV. Along the $\Gamma \rightarrow A$ direction [Fig. 3(c)] a deviation of 8.1% from the theory is found at small q, while the agreement improves to 2% at higher q values.

The remarkable agreement between the experimental and theoretical phonon dispersions is direct proof that GGA+U introduces important corrections to the interatomic forces. Calculations with GGA, without including electron correlations, result in a downshift of the dispersion relations on the energy scale by about 2 meV and a change in the slopes of the acoustic branches, leading to unacceptably large deviations from the experimental data. As a consequence, a disagreement by more than 30% between the experimental and theoretical elastic constants obtained in GGA is evidenced by Table I. Within the $4f$-core model, the acoustic branches are well described but the high-energy optical modes are strongly overestimated (see Fig. S4 from [39]).

The larger bulk modulus obtained with the GGA+U seems to contradict the typical observation that elastic parameters are reduced by the electron localization. However, in light rare earths, the localized $4f$-core model gives larger values of the bulk modulus (and volume) [24] compared to the $4f$-band model [28]. Therefore, the local Coulomb interaction (U), which induces partial localization of the $4f$ electrons, also increases the bulk modulus and gives much better agreement with the experiment than the $4f$-band calculations.

The effect of electron correlations on the lattice dynamical properties, discussed here for Nd, may be as well a general feature of the other lanthanides. For example, the experimentally observed broadening of optical modes in the PDOS of Sm, which leads to some discrepancy between experiment and theory [30], most likely has its origin in a splitting of the high-energy modes found in the Nd PDOS. This is demonstrated by a comparison of the PDOS convoluted with a Gaussian with FWHM = 1 meV for calculations with GGA and GGA+U in Fig. 1(b). At this energy resolution the splitting of the high-energy phonon branches results in an overall broadening mostly of the optical modes of the PDOS calculated with GGA+U.

In summary, we have performed a combined theoretical (DFT) and experimental (IXS) study of the lattice dynamics of

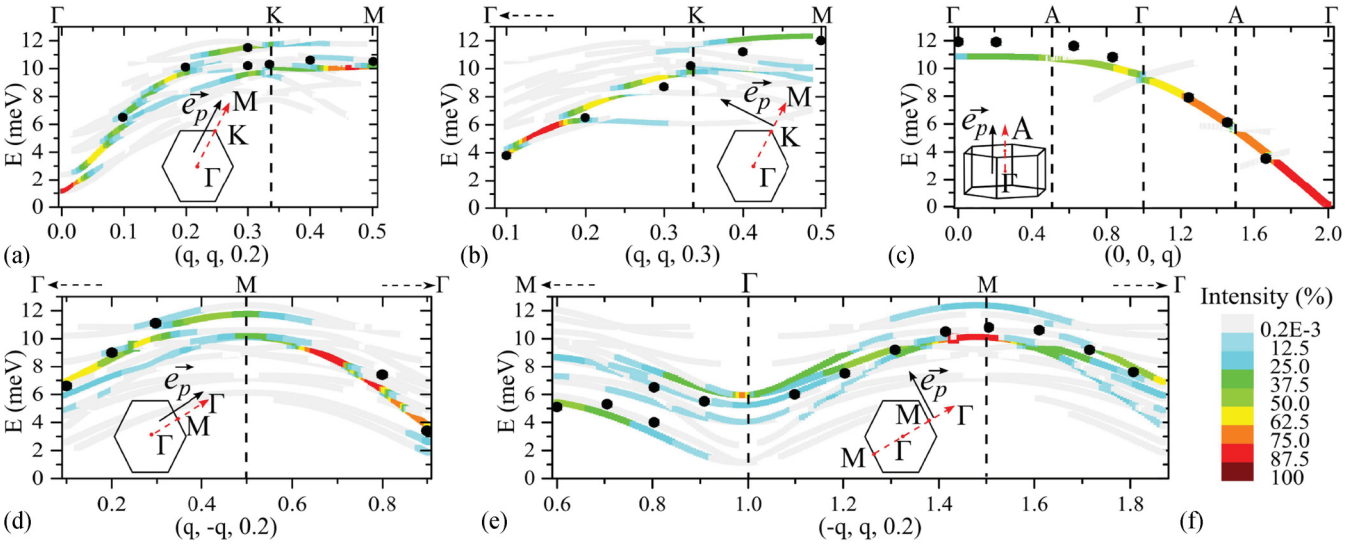

FIG. 3. Comparison between the GGA+U calculated (colored lines) and measured by IXS (black circles; error bars are comparable to the symbol size) phonon branches close to (a), (b) $\Gamma \rightarrow K \rightarrow M$, (c) along $\Gamma \rightarrow A$, and (d), (e) close to $\Gamma \rightarrow M \rightarrow \Gamma$ directions. The intensity scale is shown in (f). The directions, polarizations, and exact coordinates of the measured branches are listed in Table II. The phonon polarization vector $\vec{e}_p$ (black arrows), direction of the momentum transfer (red dashed arrows), and dhcp Brillouin zone (black hexagon/structure) are shown as insets. Details about the calculation of the intensity of the phonon branches is given in [39].

the light rare-earth element Nd. The calculations within GGA_0, GGA, and GGA+U revealed a drastic influence of the $4f$ electron correlations on the lattice dynamics of Nd. The dispersion curves obtained within GGA+U were confirmed to be correct by achieving an overall agreement of better than 7% with the IXS experimental data. The Coulomb interaction U leads to a partial electron localization reducing the screening effects of the $4f$ electrons and consequently to a very good agreement of the calculated lattice constants and elastic properties with the experimental values. This provides a better description of the properties of Nd than the fully localized $4f$-core model.

The presented results clearly demonstrate that (i) $4f$ electron correlations have a remarkable influence on the lattice dynamics of the rare-earth metals. The calculated interatomic forces and phonon energies appear to be strongly reduced and therefore erroneous if these interactions are not taken into account; and (ii) GGA+U provides a reliable description of the electronic properties and lattice dynamics of the light lanthanides.

ACKNOWLEDGMENTS

We are grateful to B. Krause, A. Weißhardt, and H. H. Gräfe for the support in the UHV-Analysis laboratory. S.S. acknowledges the financial support by the Initiative and Networking Funds of the President of the Helmholtz Association and the Karlsruhe Institute of Technology (KIT) for the Helmholtz-University Young Investigators Group "Interplay between structure and dynamics in epitaxial rare earth nanostructures," Contract No. VH-NG-625. P.P. acknowledges support by the Polish National Science Center (NCN) under Projects No. 2011/01/M/ST3/00738 and No. 2012/04/A/ST3/00331. Nd was supplied by the Materials Preparation Center, Ames Laboratory, U.S. DOE Basic Energy Sciences, Ames, IA, USA. We acknowledge ESRF-–The European Synchrotron for provision of synchrotron radiation facilities. The financial support for the UHV-Analysis laboratory via the Excellence Initiative within the project KIT-Nanolab@ANKA is acknowledged.

[1] B. Himmetoglu, A. Floris, S. de Gironcoli, and M. Cococcioni, Int. J. Quantum Chem. **114**, 14 (2014); H. Jiang, *ibid.* **115**, 722 (2015).

[2] D. Sholl and J. A. Steckel, *Density Functional Theory: A Practical Introduction* (Wiley, New York, 2009).

[3] R. M. Martin, *Electronic Structure: Basic Theory and Practical Methods* (Cambridge University Press, Cambridge, UK, 2004).

[4] R. O. Jones and O. Gunnarsson, Rev. Mod. Phys. **61**, 689 (1989).

[5] P. Ziesche, S. Kurth, and J. P. Pardew, Comput. Mater. Sci. **11**, 122 (1998).

[6] J. P. Perdew and A. Zunger, Phys. Rev. B **23**, 5048 (1981).

[7] V. I. Anisimov, J. Zaanen, and O. K. Andersen, Phys. Rev. B **44**, 943 (1991).

[8] A. D. Becke, J. Chem. Phys. **98**, 5648 (1993).

[9] W. Metzner and D. Vollhardt, Phys. Rev. Lett. **62**, 324 (1989); A. Georges, G. Kotliar, W. Krauth, and M. J. Rozenberg, Rev. Mod. Phys. **68**, 13 (1996); J. A. Bradley, K. T. Moore, M. J. Lipp, B. A. Mattern, J. I. Pacold, G. T. Seidler, P. Chow, E. Rod, Y. Xiao, and W. J. Evans, Phys. Rev. B **85**, 100102 (2012).

[10] W. Yang, Y. Zhang, and P. W. Ayers, Phys. Rev. Lett. **84**, 5172 (2000); R. Requist and O. Pankratov, Phys. Rev. B **77**, 235121 (2008); S. Sharma, J. K. Dewhurst, N. N. Lathiotakis, and E. K.

U. Gross, *ibid.* **78**, 201103 (2008); N. Helbig, N. N. Lathiotakis, and E. K. U. Gross, Phys. Rev. A **79**, 022504 (2009).

[11] V. I. Anisimov, A. I. Poteryaev, M. A. Korotin, A. O. Anokhin, and G. Kotliar, J. Phys.: Condens. Matter **9**, 7359 (1997); G. Kotliar, S. Y. Savrasov, K. Haule, V. S. Oudovenko, O. Parcollet, and C. A. Marianetti, Rev. Mod. Phys. **78**, 865 (2006).

[12] X. Dai, S. Y. Savrasov, G. Kotliar, A. Migliori, H. Ledbetter, and E. Abrahams, Science **300**, 953 (2003); B. Amadon, S. Biermann, A. Georges, and F. Aryasetiawan, Phys. Rev. Lett. **96**, 066402 (2006); H. Park, A. J. Millis, and C. A. Marianetti, Phys. Rev. B **90**, 235103 (2014); I. Leonov, V. I. Anisimov, and D. Vollhardt, Phys. Rev. Lett. **112**, 146401 (2014); K. Haule and T. Birol, *ibid.* **115**, 256402 (2015); B. Amadon and A. Gerossier, Phys. Rev. B **91**, 161103 (2015).

[13] L. V. Pourovskii, B. Amadon, S. Biermann, and A. Georges, Phys. Rev. B **76**, 235101 (2007).

[14] R. Mittal, L. Pintschovius, D. Lamago, R. Heid, K.-P. Bohnen, D. Reznik, S. L. Chaplot, Y. Su, N. Kumar, and S. K. Dhar, J. Phys.: Conf. Ser. **251**, 012008 (2010).

[15] S. Y. Savrasov and G. Kotliar, Phys. Rev. Lett. **90**, 056401 (2003).

[16] P. Piekarz, K. Parlinski, and A. M. Oleś, Phys. Rev. Lett. **97**, 156402 (2006); Phys. Rev. B **76**, 165124 (2007).

[17] U. D. Wdowik and K. Parlinski, Phys. Rev. B **75**, 104306 (2007).

[18] A. Floris, S. de Gironcoli, E. K. U. Gross, and M. Cococcioni, Phys. Rev. B **84**, 161102 (2011).

[19] U. D. Wdowik, P. Piekarz, K. Parlinski, A. M. Oleś, and J. Korecki, Phys. Rev. B **87**, 121106 (2013).

[20] S. Raymond, P. Piekarz, J. P. Sanchez, J. Serrano, M. Krisch, B. Janoušová, J. Rebizant, N. Metoki, K. Kaneko, P. T. Jochym, A. M. Oleś, and K. Parlinski, Phys. Rev. Lett. **96**, 237003 (2006).

[21] Y. Wang, L. A. Zhang, S. Shang, Z. K. Liu, and L. Q. Chen, Phys. Rev. B **88**, 024304 (2013); R. Pradip, P. Piekarz, A. Bosak, D.G. Merkel, O. Waller, A. Seiler, A.I. Chumakov, R. Rüffer, A.M. Oleś, K. Parlinski, M. Krisch, T. Baumbach, and S. Stankov, Phys. Rev. Lett. **116**, 185501 (2016).

[22] G. H. Lander and G. R. Choppin, *Handbook on the Physics and Chemistry of the Rare Earths* (North-Holland, Amsterdam, 1993).

[23] B. I. Min, H. I. J. Jansen, T. Oguchi, and A. J. Freeman, J. Magn. Magn. Mater. **61**, 139 (1986).

[24] A. Delin, L. Fast, B. Johansson, O. Eriksson, and J. M. Wills, Phys. Rev. B **58**, 4345 (1998).

[25] P. Strange, A. Svane, W. M. Temmerman, Z. Szotek, and H. Winter, Nature (London) **399**, 756 (1999).

[26] A. K. McMahan, Phys. Rev. B **72**, 115125 (2005).

[27] S. K. Mohanta, S. N. Mishra, S. K. Srivastava, and M. Rots, Solid State Commun. **150**, 1789 (2010).

[28] P. Söderlind, P. E. A. Turchi, A. Landa, and V. Lordi, J. Phys.: Condens. Matter **26**, 416001 (2014).

[29] S. Stankov, P. Piekarz, A. M. Oleś, K. Parlinski, and R. Ruffer, Phys. Rev. B **78**, 180301 (2008).

[30] O. Bauder, P. Piekarz, A. Barla, I. Sergueev, R. Ruffer, J. Lazewski, T. Baumbach, K. Parlinski, and S. Stankov, Phys. Rev. B **88**, 224303 (2013).

[31] G. Kresse and J. Furthmüller, Comput. Mater. Sci. **6**, 15 (1996); Phys. Rev. B **54**, 11169 (1996).

[32] P. E. Blöchl, Phys. Rev. B **50**, 17953 (1994); G. Kresse and D. Joubert, *ibid.* **59**, 1758 (1999).

[33] J. P. Perdew, K. Burke, and M. Ernzerhof, Phys. Rev. Lett. **77**, 3865 (1996). **78**, 1396 (1997).

[34] F. Nilsson, R. Sakuma, and F. Aryasetiawan, Phys. Rev. B **88**, 125123 (2013).

[35] D. Gryaznov, E. Heifets, and E. Kotomin, Phys. Chem. Chem. Phys. **14**, 4482 (2012).

[36] H. J. Monkhorst and J. D. Pack, Phys. Rev. B **13**, 5188 (1976).

[37] P. T. Jochym, K. Parlinski, and M. Sternik, Eur. Phys. J. B **10**, 9 (1999); P. T. Jochym and K. Parlinski, *ibid.* **15**, 265 (2000); P. T. Jochym, Computer code ELASTIC, Zenodo doi:10.5281/zenodo.18759, http://wolf.ifj.edu.pl/elastic/.

[38] K. Parlinski, Z.-Q. Li, and Y. Kawazoe, Phys. Rev. Lett. **78**, 4063 (1997); K. Parlinski, Computer code PHONON, Cracow, 2012.

[39] See Supplemental Material at http://link.aps.org/supplemental/10.1103/PhysRevB.94.014303 for a comparison of GGA, GGA+U, and GGA_0 calculated phonon dispersions and phonon DOS with experimental and optimized lattice constants, and for calculation of the intensities of the phonon branches.

[40] C. Dufour, K. Dumesnil, S. Soriano, D. Pierre, Ch. Senet, and Ph. Mangin, J. Cryst Growth **234**, 447 (2002).

[41] M. Krisch and F. Sette, *Light Scattering in Solid IX*, edited by M. Cardona and R. Merlin, Topics in Applied Physics Vol. 108 (Springer, Berlin/Heidelberg, 2007), pp. 317–370.

[42] K. A. Gschneidner, Jr., Bull. Alloy Phase Diagrams **11**, 216 (1990).

[43] W. A. Grosshans and W. B. Holzapfel, Phys. Rev. B **45**, 5171 (1992).

[44] J. D. Greiner *et al.*, J. Appl. Phys. **47**, 3427 (1976).

[45] S. Arajas and R. V. Colvin, J. Less-Common Met. **4**, 159 (1962).

[46] Similar effects of the Hubbard U parameter on the phonon dispersions and PDOS of the strongly correlated 3*d* oxides NiO and MnO were reported in Ref. [18].